

# **Groundwater controls on post-fire permafrost thaw: Water and energy balance effects**

**Samuel C. Zipper<sup>1,2</sup>, Pierrick Lamontagne-Hallé<sup>1</sup>, Jeffrey M. McKenzie<sup>1</sup>, Adrian V. Rocha<sup>3</sup>**

<sup>1</sup>Department of Earth and Planetary Sciences, McGill University, Montreal QC, Canada

<sup>2</sup>Department of Civil Engineering, University of Victoria, Victoria BC, Canada

<sup>3</sup>Department of Biological Sciences and the Global Change Initiative, University of Notre Dame, Notre Dame IN, USA

Corresponding author: Samuel C. Zipper (samuelczipper@gmail.com)

## **Key Points:**

- Ignoring groundwater flow may cause over/underestimation of the influence of thermal/hydrologic properties on post-fire permafrost thaw
- Post-fire increases in soil temperature increase both conductive and advective heat transport, leading to thicker active layer
- Lateral thaw depth variability and groundwater discharge to streams decreases following fire due to decreases in groundwater recharge

## **Abstract**

Fire frequency and severity is increasing in high latitude regions, with large impacts on the water and energy balances. However, the degree to which groundwater flow impacts the permafrost response to fire remains poorly understood and understudied. Here, we use the Anaktuvuk River Fire (Alaska, USA) as an archetypal example to investigate groundwater-permafrost interactions following fire. We identify key thermal and hydrologic parameters controlling permafrost and active layer response to fire both with and without groundwater flow, and separate the relative importance of changes to the water and energy balances. Our results show that mineral soil porosity, which influences the bulk subsurface thermal conductivity, is a key parameter controlling active layer response to fire in both the absence and presence of groundwater flow. However, neglecting groundwater flow increases the perceived importance of subsurface thermal properties, such as the thermal conductivity of soil solids, and decreases the perceived importance of hydrologic properties, such as the soil permeability. Furthermore, we demonstrate that changes to the energy balance (increased soil temperature) are the key driver of increased active layer thickness following fire, while changes to the water balance (decreased groundwater recharge) lead to reduced landscape-scale variability in active layer thickness and groundwater discharge to surface water features. These results indicate that explicit consideration of groundwater flow is critical to understanding how permafrost environments respond to fire.

## **Plain Language Summary**

While scientists know that fire often causes permafrost (areas of permanently frozen ground) to thaw, the degree to which the movement of groundwater either enhances or reduces this thawing process is not well understood. In this study, we simulate the response to permafrost to fire using models that both include and ignore groundwater flow while varying different model input datasets. Our results show that, when groundwater flow is ignored, the relative importance of soil properties associated with heat movement may be overestimated, and the importance of soil properties associated with water movement are likely to be underestimated. Additionally, we show that increased soil temperature following fire is the most important factor deepening permafrost thaw each year (also known as the ‘active layer’). However, reductions in the amount of water recharging groundwater systems decreased differences in permafrost thaw depth between upland and lowland regions of a watershed, as well as the amount of groundwater that flows into surface water features such as streams.

## **Index Terms:**

1829 Groundwater hydrology; 0475 Permafrost, cryosphere, and high-latitude processes; 0764 Energy balance; 1655 Water cycles; 1846 Model calibration

## **Keywords:**

tundra fire; Long-Term Ecological Research (LTER) network; active layer thickness; baseflow; Arctic; groundwater modeling;

## 1 Introduction

Fire frequency and severity in the Arctic is expected to increase in the future, and can have substantial impacts on permafrost, hydrology, and biogeochemistry (Flannigan et al., 2005; Hu et al., 2015). Fires increase the thickness of the active layer (the suprapermafrost layer which thaws and refreezes annually) by thinning the near-surface organic soil layer and reducing the thermal buffer between air and the subsurface, and by decreasing albedo which further increases in energy input into the subsurface (Brown et al., 2015, 2016; Iwahana et al., 2016; Kasischke & Johnstone, 2005; Rocha & Shaver, 2011b; Smith et al., 2015). Past modeling efforts studying post-fire active layer thickness have neglected the potential impacts of groundwater flow on permafrost by using one-dimensional models (Brown et al., 2015; Jiang et al., 2015b; Treat et al., 2013; Yi et al., 2009; Zhang et al., 2003, 2015; Zhuang et al., 2002). One-dimensional models implicitly assume that changes to the energy balance dominate post-fire permafrost response, and that soil thermal properties are most important control of permafrost response to fire (Jiang et al., 2012, 2015b; Yi et al., 2009).

In contrast, however, field research suggests that hydrologic properties such as drainage patterns and soil textural properties influence permafrost response to fire (Connon et al., 2015; Kasischke et al., 2007; Minsley et al., 2016), implying that hydrological processes may be an important control on post-fire permafrost thaw. Increased subsurface hydrological connectivity, which is associated with thickening active layers, has been shown to lead to positive feedbacks on permafrost thaw by increasing advective heat transport via groundwater flow, though this has not been studied in the context of fire (Bense et al., 2009, 2012; Connon et al., 2014; Kurylyk et al., 2016; McKenzie & Voss, 2013; Walvoord et al., 2012). Such processes could result in a positive post-fire feedback on permafrost degradation. However, the role of groundwater flow in mediating post-fire changes in active layer thickness but are not well understood due to a lack of available data in high-latitude regions, and no previous modelling work has investigated the importance of fire-induced feedbacks between groundwater flow on permafrost degradation.

To address this knowledge gap, this study explores the question, *how does groundwater flow impact permafrost response to fire?* We answer this question using an archetypal modeling approach, which simplifies a real-world domain to test hypotheses in a generalizable process-based manner, rather than constructing a site-specific model. Our archetypal models are driven by field observations from three sites along a burn severity gradient (i.e. Severe, Moderate, and Unburned) within the largest recorded tundra fire in Alaska's history. During this time, the 3 sites exhibited a large gradient in soil thermal dynamics that allowed us to address three tractable sub-questions: (1) what are the key thermal and hydrologic properties governing post-fire active layer thickness?; (2) how do these change in the presence or absence of groundwater flow?; and (3) what are the relative impacts of post-fire changes to the water balance and energy balance on active layer thickness and groundwater discharge to surface water? As fire effects are superimposed on a warming trend which is already contributing to permafrost thaw across the Arctic, understanding the response of permafrost and subsurface hydrology to fire is key to predicting and planning for future change in terrestrial and aquatic ecosystems (Hu et al., 2015; Lique et al., 2016; Walvoord & Kurylyk, 2016; Wrona et al., 2016).

## 2 Methodology

### 2.1 Anaktuvuk River Fire

To investigate these questions, we focus on the Anaktuvuk River Fire (ARF). The ARF burned ~1000 km<sup>2</sup> of Alaska's North Slope from July through October of 2007, making it the largest recorded tundra fire in Alaska's history (Jones et al., 2009). Consequently, the ARF had dramatic impacts on energy, water, carbon, and nutrient cycling (Bret-Harte et al., 2013; De Baets et al., 2016; Jiang et al., 2015a, 2017; Mack et al., 2011; Rocha & Shaver, 2011a). Importantly, the ARF may be an analog for a future Arctic in which warmer temperatures and shrub ecosystems favoring fire expand, though future climate impacts on Arctic fire regimes are highly uncertain (Higuera et al., 2008; Hu et al., 2010, 2015). This makes the ARF a broadly instructive example for considering the impacts of tundra fire on permafrost environments.

In the present study, we use three sites across a burn gradient which were instrumented with eddy covariance towers in June 2008, which we will refer to as Unburned (UB; 68.99°N, 150.28°W), Moderate Burn (MB; 68.95°N, 150.21°W), and Severe Burn (SB; 68.93°N, 150.27°W). The UB site is tundra tussock which was not affected by the fire; the MB site is a mix of partially and completely burned areas; and all vegetation was burned at the SB site (Rocha & Shaver, 2009, 2011a). Previous research documented several thermal and hydrological changes in response to the ARF. A decrease in soil organic layer thickness and albedo led to higher summer soil temperature at the MB and SB sites relative to UB baseline; and an increase in evapotranspiration due to surface ponding following the loss of soil organic matter (Jiang et al., 2015b; Rocha & Shaver, 2011b).

### 2.2 Modeling approach

To test our hypotheses (Section 1), we used a suite of numerical model simulations that are representative of the ARF sites. Our guiding principle in model design was that of parsimonious archetypal modeling, or making a groundwater flow model in “the simplest way possible that captures the most important overall behavior” (Voss, 2011b, p. 1456). We use the modified version of the SUTRA numerical model (Voss & Provost, 2010) described in McKenzie et al. (2007) and McKenzie & Voss (2013). The modified model simulates saturated groundwater flow including freeze/thaw processes, which impact subsurface hydrologic and thermal properties based on the relative composition of three materials: liquid water, solid water (ice), and matrix material (soil solids).

Permeability is defined for the solid matrix material, and reduced as a function of liquid pore-water saturation using a relative permeability scaling coefficient. This coefficient is multiplied by the solid matrix permeability to obtain the effective permeability. We simulated saturated groundwater flow only, meaning that liquid pore-water saturation decreases when ice forms due to pore-water freezing. In our simulations, relative permeability decreased linearly as a function of decreasing liquid pore-water saturation to a minimum value of  $10^{-8}$ . The onset of pore water freezing at a node occurs when temperature drops below 0 °C, and the proportion of frozen pore water increases linearly until a threshold temperature is reached (set here as -2 °C; McKenzie & Voss, 2013). At and below this threshold temperature, liquid water content is equal to a minimum allowed residual liquid water content (set here as 1% of pore space). Parameter values used in our simulation are defined in Table 1. For a full description of the model the reader is referred to McKenzie et al. (2007) and McKenzie & Voss (2013).

**Table 1.** Thermal and hydrologic properties of the numerical model. Parameters where value varied between 1D and 2D simulations are noted. Bold values are varied in sensitivity analysis (Section 2.2.3).

Parameter	Value	Source/Notes
<i>Discretization</i>		
Width (x dimension)	1D: 5 m 2D: 200 m	200 m is typical watershed half-width for Anaktuvuk River Fire region
Height (y dimension)	1D: 20 m 2D: 25 m to 20 m	Model height based on thermal bottom boundary condition (Section 2.2.2)
Slope	1D: 0% 2D: 2.5%	(Rocha & Shaver, 2011b)
Model Discretization (x)	5 m	
Model Discretization (y)	0.03 m (top) to 2.0 m (bottom)	
Number of Nodes/Elements	1D: 453/300 2D: 4961/4800	
Model Duration	6935 days	19 years (1998-2016), ignoring leap years
Model Timestep	1 day	
<i>Thermal Properties</i>		
<b>Organic soil solid thermal conductivity</b>	<b>0.25 to 0.69 W m<sup>-2</sup> °C<sup>-1</sup></b>	Literature values for peat (Jafarov et al., 2013; Kurylyk et al., 2016; McKenzie et al., 2007; Treat et al., 2013)
<b>Mineral soil solid thermal conductivity</b>	<b>1.40 to 1.84 W m<sup>-2</sup> °C<sup>-1</sup></b>	Mean value from (Kurylyk et al., 2016) (1.62 W m <sup>-2</sup> K <sup>-1</sup> ) +/- half of range of organic soil thermal conductivity
Organic soil solid specific heat	1920 J kg <sup>-1</sup>	(McKenzie et al., 2007)
Mineral soil solid specific heat	870 J kg <sup>-1</sup>	(Campbell & Norman, 2000)
Liquid water thermal conductivity	0.6 W m <sup>-2</sup> °C <sup>-1</sup>	(McKenzie & Voss, 2013)
Liquid water specific heat	4182 J kg <sup>-1</sup>	(McKenzie & Voss, 2013)
Ice thermal conductivity	2.13 W m <sup>-2</sup> °C <sup>-1</sup>	(McKenzie & Voss, 2013)
Ice specific heat	2108 J kg <sup>-1</sup>	(McKenzie & Voss, 2013)
<i>Hydrologic Properties</i>		
<b>Organic soil vertical permeability</b>	<b>10<sup>-15</sup> to 10<sup>-9</sup> m<sup>2</sup></b>	Literature values for peat (Jiang et al., 2015b; Naasz et al., 2005; Schwärzel et al., 2006; da Silva et al., 1993; Zhang et al., 2010)
<b>Mineral soil vertical permeability</b>	<b>10<sup>-15</sup> to 10<sup>-11</sup> m<sup>2</sup></b>	(Carsel & Parrish, 1988) mean for silt loam soil +/- 2 orders of magnitude
Vertical/Horizontal Permeability Ratio	0.1	
<b>Organic soil porosity</b>	<b>0.60 to 0.80</b>	Volumetric water content measurements (Rocha et al., 2008a, 2008b, 2008c; Romanovsky et al., 2017)
<b>Mineral soil porosity</b>	<b>0.35 to 0.55</b>	(Carsel & Parrish, 1988) mean for silt loam soil +/- 0.10
<i>Soil Freezing Properties</i>		
Soil freezing function	Linear	(McKenzie & Voss, 2013)
Minimum liquid saturation	0.01	(McKenzie & Voss, 2013)
Temperature below which minimum liquid saturation occurs	-2 °C	(McKenzie & Voss, 2013)
Relative permeability function	Linear	(McKenzie & Voss, 2013)
Minimum relative permeability	1 x 10 <sup>-8</sup>	(Kurylyk et al., 2016)

### 2.2.1 Domain and discretization

We created two separate domains intended to isolate the impact of groundwater flow on permafrost response to fire: a one-dimensional (1D) vertical column in which no groundwater flow occurs; and a two-dimensional (2D) watershed cross-section with groundwater flow induced by a sloping land surface and a stream with an underlying talik at the downstream end of the domain (Figure 1). The archetypal domains are not intended to perfectly recreate the Anaktuvuk River field sites, but rather to isolate the impact of groundwater along the dominant hydrogeologic flow field (typically perpendicular to groundwater divides such as streams), thus allowing for a process-based exploration of fire impacts on groundwater-permafrost interactions (Voss, 2011a, 2011b). For both domains, our conceptual model was that of a two-layer (organic soil and mineral soil), fully saturated subsurface with homogeneous hydrologic and thermal properties within each layer. We discretized the model into 120 vertical layers, increasing in thickness from 0.03 m at the land surface to 2.0 m at the bottom of the domain. Since both nodes and elements are required to simulate water and heat transport, a true one-dimensional soil column is not possible; therefore, the 1D domain was three nodes (two elements) wide, with boundary conditions on the right and left sides and results were taken from the middle column of nodes. The 2D domain was 41 nodes (40 elements) wide, with a uniform node spacing of 5 m. The land surface of the 2D domain sloped from 25 m (at  $x=0$  m) to 20 m (at  $x=200$  m), to produce a 2.5% slope typical of the ARF region (Rocha & Shaver, 2011b). At the right edge of the 2D domain, we used a boundary condition representative of a simplified stream with underlying talik (see Section 2.2.2).

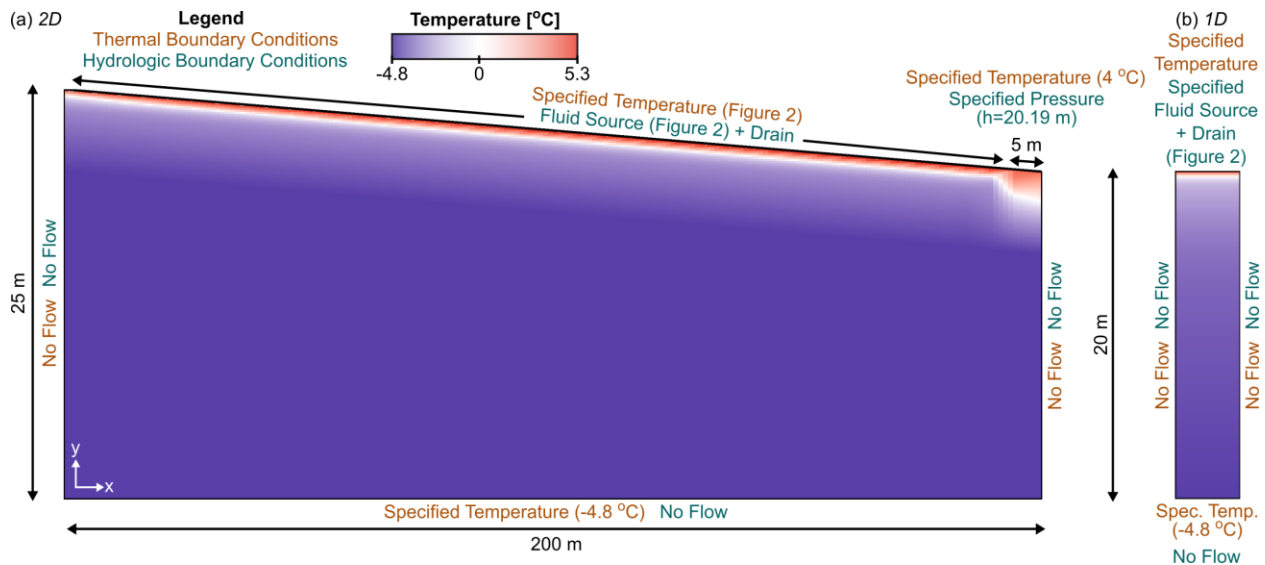


**Figure 1.** Model domain for (a) 2D domain, which includes lateral groundwater flow; and (b) 1D domain, which ignores lateral groundwater flow. Colors show simulated temperature for unburned (UB) site on September 1, 2009.

In total, we constructed 6 unique model domains based on a factorial combination of model dimensionality (1D and 2D) and burn severity (UB, MB, and SB), which differed in the relative thickness of the organic and mineral soil layers (Table 2). In the following sections, we describe the boundary conditions (Section 2.2.2) which were applied to each domain to explore parameter sensitivity (Section 2.2.3) and separate the impacts of changes in the water and energy balances (Section 2.3).

### 2.2.2 Inputs and boundary conditions

Model thermal and hydrologic boundary conditions for each domain were temporally constant on the bottom, left, and right sides (Figure 1). While specified heat flux bottom boundary conditions are typically used for studies of permafrost-groundwater interactions (Evans & Ge, 2017; Kurylyk et al., 2016; McKenzie & Voss, 2013; Wellman et al., 2013), the focus of our study was exclusively shallow processes occurring in the active layer, and preliminary simulations indicated that simulating a subpermafrost aquifer did not impact our results over the decadal timescale examined here. Therefore, we decided to use a specified temperature bottom boundary condition at the zero annual temperature amplitude depth to reduce the size of the model domain and permit a more detailed sensitivity analysis (Section 2.2.3). We defined this temperature (-4.8 °C) and bottom boundary depth (20 m) based on ground temperature measurements at the Seabee Borehole (69.38°N, 152.18°W; 87 km from ARF sites), part of the Global Terrestrial Network for Permafrost database (Clow, 2014). Thermal boundary conditions were zero heat flux on the right and left edges of the domain. Hydrologic boundary conditions were no-flow on the bottom, left, and right sides.

The upper thermal boundary condition was time-varying specified temperature based on daily soil temperature measurements from each of the three burn severity sites at 5 cm beneath the land surface. By using subsurface soil temperature as model input, this boundary condition accounts for changes to the energy balance at the land surface, e.g. due to changes in albedo and vegetation. From the time of flux tower installation at the ARF sites (June 2008) through the end of 2016, we used measured daily soil temperature at 0.05 m depth from each ARF site (Figure 2a) (Shaver and Rocha, 2015a-o). For the 2009-2016 period, there were 749, 480, and 343 days without data at the UB, MB, and SB sites, respectively, which primarily occurred during the winter. We gap-filled missing soil temperature data for the post-fire period using linear interpolation (for gaps  $\leq 7$  days) or the average soil temperature for that day of year and burn severity (for gaps  $> 7$  days).

The upper hydrologic boundary condition was a specified fluid source to the top layer of nodes representing groundwater recharge. Generalized pressure (or drain) boundary conditions were also implemented along the top boundary condition to prevent overpressuring (Evans & Ge, 2017). Groundwater recharge was estimated using a set fraction of daily combined rainfall and snowmelt from a temperature-based snowpack model (Walter et al., 2005) implemented within the *EcoHydrology* R package (Fuka et al., 2014) and driven using daily meteorological data from the Toolik Field Station (Environmental Data Center Team, 2017). We used 20% of combined rainfall and snowmelt as a fluid source for the UB site, with a 40% reduction (=12% of combined rainfall and snowmelt) at the MB and SB sites corresponding to the increase in evapotranspiration observed at these sites (Rocha & Shaver, 2011b). As annual evapotranspiration at the burned sites was consistently ~40-45% higher than the UB site over the 2008-2016 period studied, we do not consider the healing of the soil organic layer as an important factor in controlling differences in groundwater recharge; this occurs over longer timescales than the sub-decadal analysis performed here, and these effects are likely smaller than the large uncertainty in precipitation estimates in tundra settings (Liljedahl et al., 2017). In the 2D domain, the rightmost 10 m of the domain were specified pressure nodes at the land surface with a hydraulic head corresponding to 20.175 m and specified temperature of 4 °C, intended to represent a river or streambed with an underlying talik. We take outflow from these specified pressure nodes to represent groundwater discharge to surface water.

Initial pressure and temperature conditions for both 1D and 2D simulations were defined using a sequential spin-up approach. First, we used a steady-state simulation to estimate reasonable pressure and temperature fields to use as initial conditions for transient simulations. In the steady-state simulations, the upper hydrologic boundary condition was a specified pressure of 0 pa (indicating a water table at the land surface) with a temperature of  $-8.43\text{ }^{\circ}\text{C}$  (the mean annual soil temperature at the UB site). Following the steady-state simulations, transient simulations were run from 1998-2007 with time-varying specified temperature and fluid source upper boundary conditions to allow the system to equilibrate to pre-fire conditions. During the 1998-2007 spin-up period prior to the installation of monitoring equipment at the ARF, we defined the upper thermal boundary conditions using daily soil temperature measurements at 0.087 m depth from the Toolik Soil Climate Research Station (Romanovsky et al., 2017). We then implemented the three different burn severity boundary conditions for the 2008-2016 period using data from the ARF sites (Figure 2).

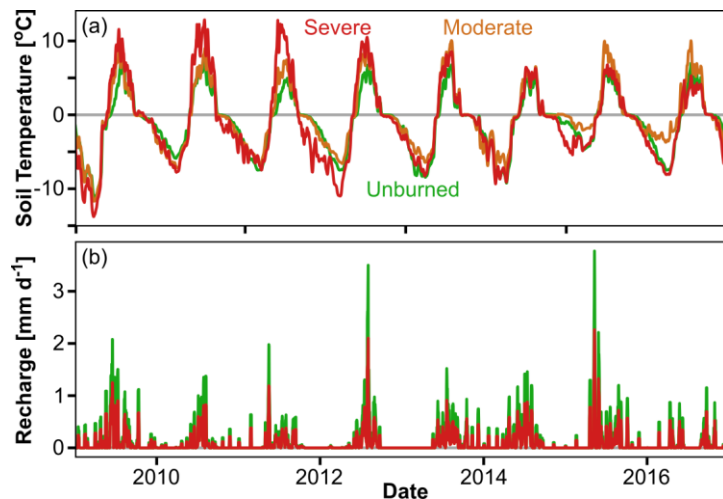


**Figure 2.** Upper boundary conditions applied to groundwater flow model at ARF sites. (a) Soil temperature, and (b) groundwater recharge inputs (same colors as (a)). In (b), Severe and Moderate inputs are the same.

While post-fire data were available for the 2008-2016 period, we elected to exclude 2008 results from analysis because the flux towers were not installed until June 2008. Therefore data from the first ~half of 2008 (including the critical spring snowmelt period) are gap-filled and considered less accurate as groundwater model inputs.

### 2.2.3 Sensitivity analysis and model evaluation

To examine the sensitivity of modeled active layer thickness to different thermal and hydrologic parameters under groundwater flow (2D) and no groundwater flow (1D) conditions, we conducted 5000 simulations while varying parameters using a Latin Hypercube Sample design for each combination of dimensionality (1D and 2D) and the burn severity endmembers (UB and SB), for 20,000 simulations total. We varied six parameters (Table 1) representing both hydrological and thermal characteristics of the subsurface: permeability, thermal conductivity, and porosity of the organic and mineral soil layers. Sampling used a uniform input distribution for each parameter, with permeability log-transformed prior to sampling.

Output from each simulation was daily temperature at each node, which we used to calculate daily thaw depth for comparison with field observations (Rocha & Shaver, 2015). For the 2D domain, we used thaw depth from the center of the domain ( $x=100\text{ m}$ ) for comparison



with field measurements to minimize potential edge-effects of the no-flow boundary conditions at the left and right edges of the domain and the talik at the right edge. As noted in Section 2.2, we employed an archetypal modeling approach using a simplified domain to isolate key processes of interest (fire-induced changes to the water and energy balance). Therefore, the comparison with thaw depth measurements is intended to provide confidence that our model is representing active layer development at the Anaktuvuk River field site in a reasonable manner, but we are not intending to build a groundwater flow model specific to each site. Thaw depth is a particularly valuable measurement for model evaluation in permafrost settings, as it integrates soil temperature through and below the active layer.

For a quantitative metric of model performance, we used the Kling-Gupta Efficiency (KGE) (Gupta et al., 2009) as implemented in the *hydroGOF* package for R (Zambrano-Bigiarini, 2014). KGE decomposes the widely-used Nash-Sutcliffe Efficiency (Nash & Sutcliffe, 1970) to provide both an overall fit ( $-\infty$  to 1) between observed and simulated timeseries, as well as separate measures of correlation ( $r$ ), bias ( $\beta$ ), and variability ( $\alpha$ ); a value of 1 corresponds to a perfect fit for both overall KGE and each decomposed metric. Given that our domain completely refreezes each winter, the maximum thaw depth for each year is equal to active layer thickness.

The relative importance of each parameter to total variability in active layer thickness and KGE was calculated separately for 1D and 2D cases using a generalized additive model (GAM) approach, as implemented in the *mgcv* package for R (Wood, 2003, 2011, 2017). GAMs are a type of generalized linear model integrating smoothing functions which are well-suited for nonlinear interactions between predictor and response variables. To estimate uncertainty, we used a bootstrapping approach in which we randomly sampled 75% of the simulation output 100 times to fit GAM models (Serbin et al., 2014; Zipper et al., 2016, 2017b; Zipper & Loheide, 2014). The proportion of variance explained by each parameter for each sample was calculated as the difference in deviance for a GAM excluding that parameter from the deviance in a GAM including all parameters, relative to the deviance from a null model.

Results from the sensitivity analysis were also used for model calibration and validation. We selected the parameters with the highest combined KGE between the UB and SB sites in which KGE at both sites was greater than 0.5. Calibrated model parameters were selected separately for the 1D and 2D domains. These calibrated parameters were then used to construct 1D and 2D models of the MB site for model validation.

### 2.3 Separating water and energy effects

To separate the effects of changes to the water and energy balance on permafrost thaw and active layer thickness, we conducted two additional simulations on the SB domain (Table 2). The first, which is intended to isolate the effects of fire-induced changes in the water balance on permafrost thaw, combined recharge from the SB site with soil temperature from the UB site (SB<sub>W</sub>). The second was intended to isolate the effects of post-fire changes in the energy balance, and combined recharge from the UB site with soil temperature from the SB site (SB<sub>E</sub>).

**Table 2.** Scenarios simulated for water and energy balance analysis.

Scenario	Purpose	Recharge Input	Temperature Input	Organic Layer Thickness [m]
Unburned [UB]	Model calibration	Unburned ARF site	Unburned ARF site	0.18
Moderate Burn [MB]	Model validation	Moderate burn ARF site	Moderate burn ARF site	0.12
Severe Burn [SB]	Model calibration	Severe burn ARF site	Severe burn ARF site	0.09
Severe-Recharge Change Only [SB <sub>w</sub> ]	Isolate water balance change effects	Severe burn ARF site	Unburned ARF site	0.09
Severe-Temperature Change Only [SB <sub>E</sub> ]	Isolate energy balance change effects	Unburned ARF site	Severe burn ARF site	0.09

### 3 Results

#### 3.1 Parameter sensitivity analysis

When groundwater is neglected (1D domain), active layer thickness is most responsive to changes in porosity of the mineral soil. There is a strong positive correlation between mean annual active layer thickness and porosity, which controls the bulk thermal conductivity of the subsurface (Figure 3a, top row). Comparing all parameters, variability in mineral soil porosity explains 72.9% (UB) and 90.9% (SB) of variability in active layer thickness (Figure 3b, top row). Soil thermal conductivity has a secondary effect on mean annual active layer thickness in the 1D simulations, with the relative importance of organic and mineral soil depending on burn severity (Figure 3, top row). At the UB site, the solid thermal conductivity of the organic soil layer explains 23.5% of variability in active layer thickness, while <1% of variability can be attributed to solid thermal conductivity of the mineral soil (Figure 3b, top row). In contrast, at the SB site, the relative importance of these two layers is reversed: mineral soil solid thermal conductivity contributes 5.6% of variability in active layer thickness, while organic soil solid thermal conductivity explains 3.0%. The greater influence of mineral soil properties at the SB site can be attributed to changes in the thickness of the organic soil layer following fire: the SB organic layer thickness is 50% that of the UB site (Table 2), thereby decreasing the relative influence of organic soil properties. The remaining properties evaluated (porosity of the organic layer, and permeability of both the mineral and organic layers) have a negligible effect on active layer thickness in the 1D domain (Figure 3, top row).

When lateral groundwater flow is simulated (2D domain), modeled sensitivity to hydrologic properties increases; permeability of both the organic and mineral layers exert a strong influence over modeled active layer thickness (Figure 3, bottom row). Permeability of the organic soil layer explains 56.2% (UB) and 8.8% (SB) of variability in active layer thickness and the permeability of the mineral soil layer contributes 6.8% (UB) and 27.2% (SB) of variability. Active layer thickness is also positively correlated with mineral soil porosity, which explains 9.7% (UB) and 44.4% (SB) of variability. The solid thermal conductivity of the mineral soil layer has a tertiary effect on active layer thickness, explaining 2.7% of variability, while the effects of all other properties are <1%. Comparing between burn severities, the relative importance of organic soil properties is higher at the UB site compared to the SB site in both 1D and 2D domains due to the thicker organic layer at the UB site. There is also greater spread in active layer thickness results for the 2D domain compared to the 1D domain (Figure 3a), despite the same number of total model parameters, because thaw depth is sensitive to more parameters when groundwater flow is included (Figure 3b).

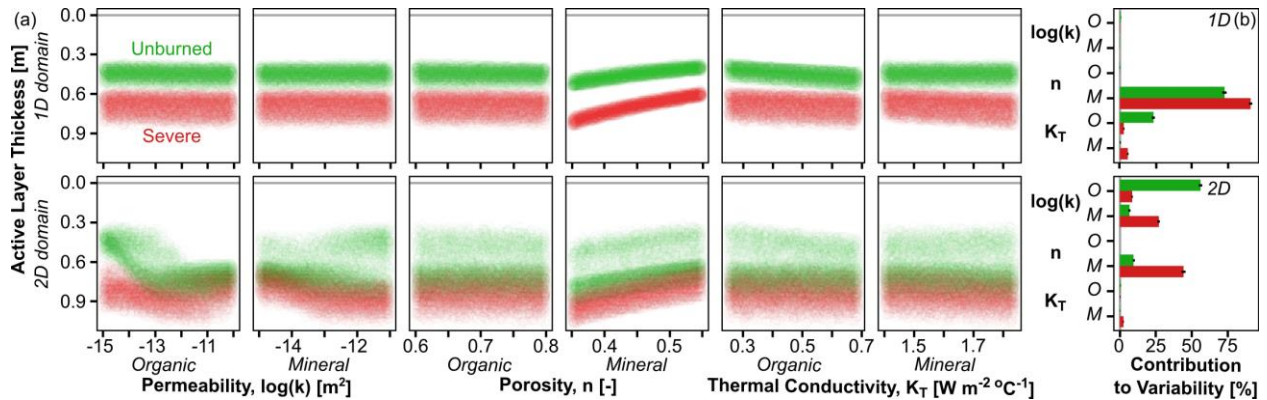


**Figure 3.** Sensitivity analysis showing active layer thickness response to thermal and hydrologic parameters. (a) Response of active layer thickness (averaged from all post-fire years) to variability in each parameter for (top row) 1D and (bottom) 2D domains. Each point represents one simulation from a 5000-sample sensitivity analysis. Note that the y-axis is reversed to match the orientation of Figure 2. (b) Relative contribution to observed active layer thickness variability for each parameter in (top) 1D and (bottom) 2D domains. ‘O’ and ‘M’ labels correspond to Organic and Mineral, respectively, and colors are the same as in (a). Bar length is the mean and line shows the minimum/maximum confidence interval based on 100-sample bootstrapped analysis. Combined contributions may exceed 100%.

The impacts of groundwater on parameter sensitivity is also evident when evaluating model performance using KGE (Figure 4). In the 1D simulations, KGE is most sensitive to changes in organic thermal conductivity (59.6% of variability), mineral soil porosity (32.6%), and mineral soil thermal conductivity (21.3%); all other parameters explain <2% of total variability in KGE. In the 2D domain, mineral soil porosity and permeability are the dominant controls (25.2% and 23.7%, respectively), followed by organic permeability (10.8%); all other parameters explain <2% of variability in KGE. In reality, one would expect porosity and permeability to be related to each other; therefore, our results shed light on the relative importance of these two coupled factors.

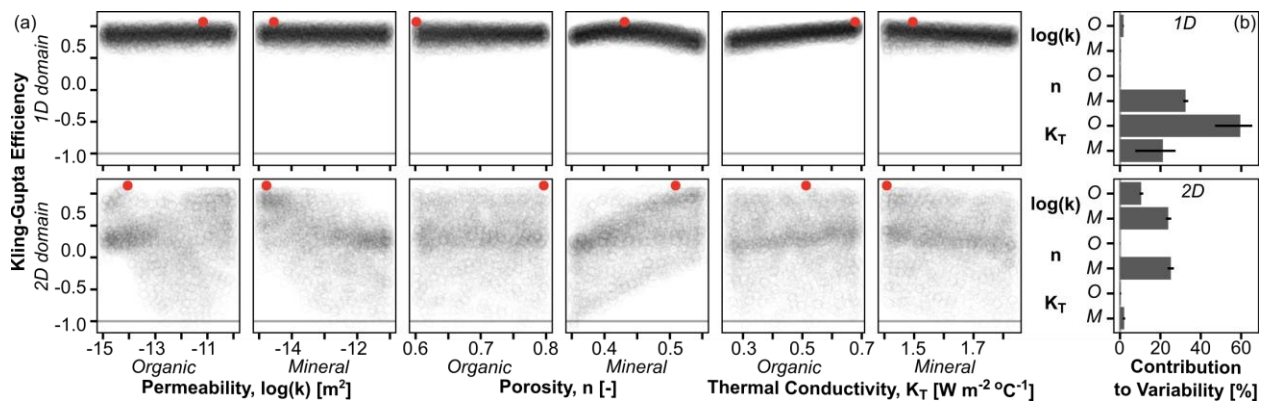


**Figure 4.** Sensitivity analysis showing model fit to observations as a function of thermal and hydrologic properties. (a) Response of mean Kling-Gupta Efficiency (Gupta et al., 2009) to variability in each parameter for (top row) 1D and (bottom) 2D domains. Each point represents one simulation from a 5000-sample sensitivity analysis. The red points show the calibrated parameters for 1D and 2D domains (Section 2.2.3), which are plotted in Figure 4. (b) Relative contribution to observed KGE variability for each parameter in (top) 1D and (bottom) 2D domains. ‘O’ and ‘M’ labels correspond to Organic and Mineral, respectively, and colors are the same as in (a). Bar length is the mean

and line shows the minimum/maximum confidence interval based on 100-sample bootstrapped analysis. Combined contributions may exceed 100%.

### 3.2 Comparison to thaw observations

Using the results of the sensitivity analysis, we defined calibrated model parameters for the 1D and 2D domains. For each domain, we selected the set of parameters that produced the best KGE averaged between the UB and SB sites (red dots in Figure 4). We then simulated the MB site as a validation test (Figure 5). Given that both mineral soil porosity and permeability are linear trends with the calibrated parameters near one end, it may be argued that increasing the range of variability would better reproduce observations by identifying the point at which model performance peaks. However, given that the sampling fully encompasses a reasonable range of values for the silt loam soil type observed at the site (Carsel & Parrish, 1988; Romanovsky et al., 2017), we elected to not further expand the sensitivity analysis to avoid model overfitting.

Overall, both 1D and 2D calibrated models performed well for the calibration and validation sites ( $KGE > 0.65$ ). At the SB site, modeled thaw depth was underpredicted in later years, particularly 2016. This is associated with a notable decrease in annual soil temperature amplitude at the SB site, which behaves similarly to the UB site by the end of the simulation period (Figure 2). However, the SB site still has the highest daily soil amplitude (not shown), indicating that subdaily thermal dynamics may be a key control on thaw depth not included in our modeling approach. Validation performance was weaker for the 1D domain than the 2D domain, primarily due to overpredicting thaw depth ( $\beta = 1.093$ ) and variability ( $\alpha = 1.284$ ) in the 1D domain. Model performance assessed using KGE is better for the 2D calibrated model than the 1D calibrated model at all sites, potentially resulting from lateral groundwater flow in the 2D model (Section 3.1).

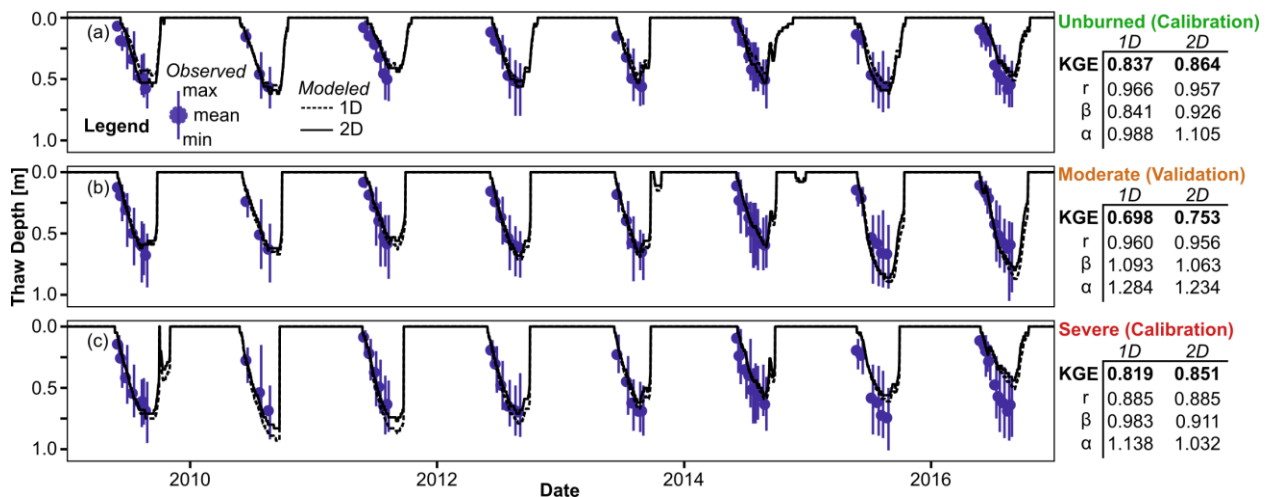


**Figure 5.** Model calibration and validation results for (a) Unburned, (b) Moderate Burn, and (c) Severe Burn sites. Fit statistics are the overall Kling-Gupta Efficiency (KGE), as well as the decomposed KGE  $r$  (measure of correlation; Pearson coefficient),  $\beta$  (measure of bias; ratio of means of simulated to observed values), and  $\alpha$  (measure of variability; ratio of standard deviations of simulated to observed values) parameters (Gupta et al., 2009).

### 3.3 Response to water and energy balance changes

Following fire, active layer thickness and thaw depth variability increase substantially. The four scenarios used to separate water and energy balance effects fall into two groups: scenarios with soil temperature inputs from the Severe Burn site (SB and SB<sub>E</sub>) have deeper thaw

(Figure 6a,c) and more variability (Figure 6b,d) than scenarios with soil temperature from the Unburned Site (UB and SB<sub>w</sub>). These dynamics are comparable in both the absence (1D) and presence (2D) of groundwater flow and indicate that post-fire changes in active layer thickness are driven primarily by changes to the energy balance. However, these changes are relatively short-lived; by 2014 (7 years after the fire), seasonal patterns of permafrost thaw and active layer thickness are comparable across all simulations, as temperature at the UB and SB sites are comparable (Figure 2).

Field measurements also show that the relative variability in thaw depth is highest at the unburned site and decreases as a function of burn severity (Figure 7b-c). The coefficient of variation (C.V.) of thaw depth measurements is 13.4% greater at the UB site compared to the SB site (0.55 vs 0.48), with MB occupying an intermediate position (Figure 7b). Temporal patterns in thaw depth variance are consistent across sites, with the largest C.V. early in the summer when mean thaw depth is lowest, and a decreasing C.V. as time goes on (Figure 7c). Thus, while previous work documented an increase in thaw depth at these sites following fire (Rocha & Shaver, 2011b), relative variability in active layer thickness decreases due to fire in observed data, consistent with observed decreases in lateral thaw gradients shown in simulation results (Figure 7a).

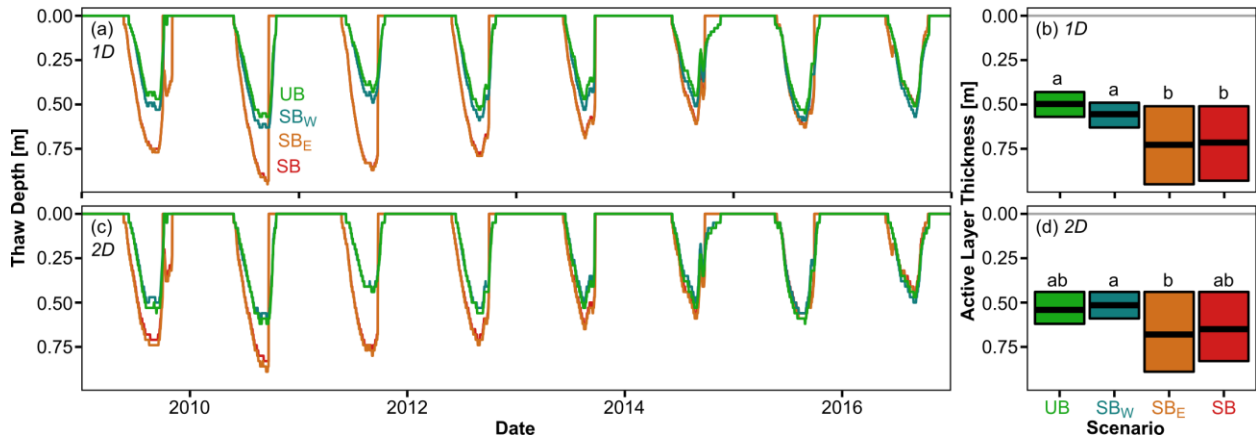


**Figure 6.** Comparison of daily thaw depth for different water and energy balance scenarios showing dominant effect of temperature. (a) Timeseries of thaw depth for different scenarios in 1D domain. Names correspond to Table 2. (b) Boxplot showing range and mean of active layer thickness for each scenario in 1D domain. Different letters denote significantly different means ( $p < 0.05$ ) between scenarios, as tested using the Tukey Honest Significant Differences test. (c) Thaw depth for different scenarios with 2D domain; (d) range and mean of active layer thickness for 2D domain.

The impacts of changes to the water and energy balance on active layer thickness also vary as a function of watershed position, and are driven by groundwater flow (Figure 7a). In all scenarios including groundwater flow (2D domain), permafrost response varies along a gradient, with thinner active layers in the uplands portion of the domain and thicker active layers in the lowland portion of the domain. Lateral thaw depth variability is largest in the scenarios without changes in the water balance due to fire: in the UB scenario active layer thickness is 0.24 m greater in the lowland region ( $x=180$  m) compared to the upland region ( $x=20$  m), a 57% increase, followed by the SB<sub>E</sub> simulation (30% increase). Reductions in groundwater recharge due to fire decrease the degree of active layer thickness variability over the domain and reduce the difference between uplands and lowland regions to 26% in the SB<sub>w</sub> scenario and 23% in the SB scenario.

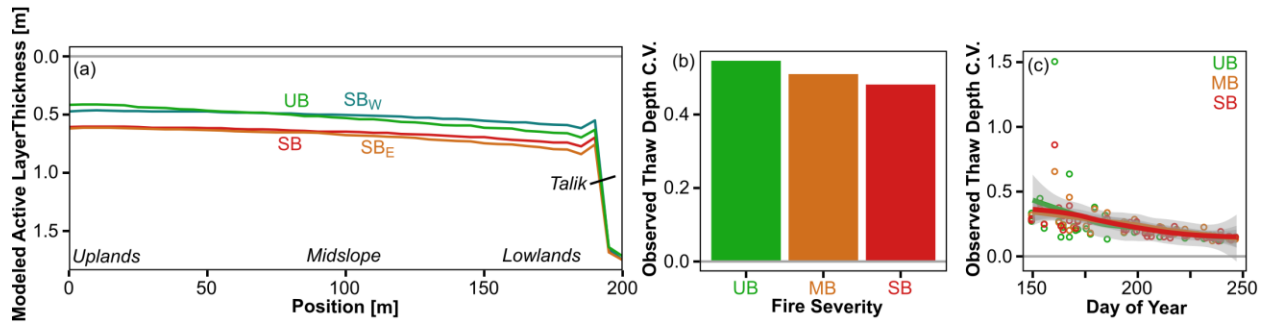


**Figure 7.** (a) Cross-section of modeled mean annual active layer thickness for each 2D water and energy balance scenario (colored lines). The region on the far-right is perennially unfrozen talik. Names correspond to Table 2. Italics denote different regions referred to in the text. (b) Coefficient of variation (C.V.) for thaw depth observations group by site and day of year for 2009-2016. (c) C.V. of thaw depth for each site by day of year across entire 2009-2016 period.

### 3.4 Groundwater discharge to surface water features

Fire may impact groundwater discharge to surface water features (e.g. rivers and streams) by changing both the supply of water (via altered recharge) and the transmissivity of the subsurface (via altered active layer thickness). Here, fire led to an approximately 50% reduction in the quantity of water released from groundwater to surface water, with mean annual discharge decreasing from 3.78 m<sup>3</sup> in the UB scenario to 1.91 m<sup>3</sup> in the SB scenario (Figure 8). This decrease is due primarily to reduced groundwater recharge following fire: the lowest observed mean annual discharge (1.83 m<sup>3</sup>) occurs in the SB<sub>W</sub> scenario, when only groundwater recharge changes, while there is a slight reduction in mean annual discharge when only soil temperature changes (3.26 m<sup>3</sup> in the SB<sub>E</sub> scenario). However, there was no observed shift in the timing of groundwater discharge to streams in either the onset of groundwater discharge in the spring or the day of peak discharge.

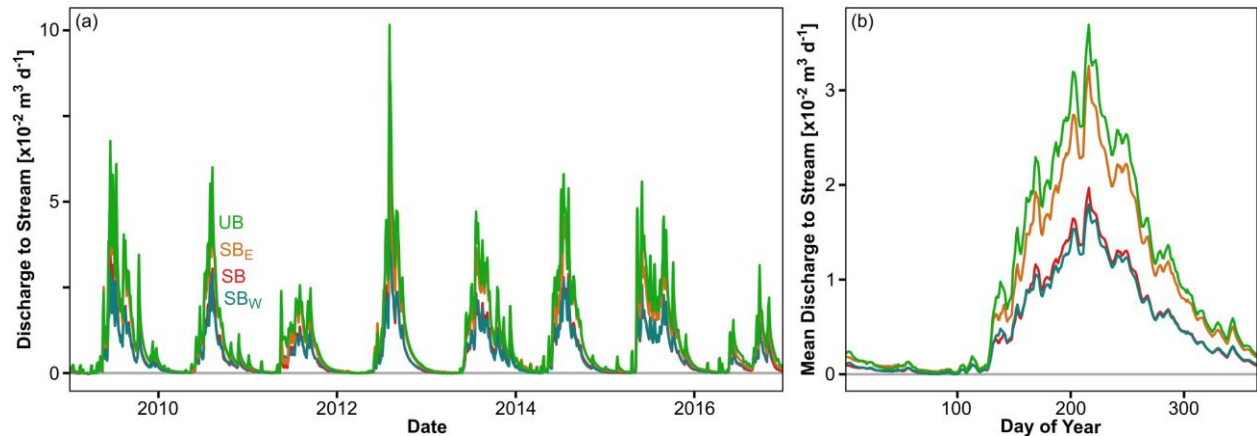


**Figure 8.** Discharge at specified pressure nodes representing stream for each 2D water and energy balance scenario (colored lines) for (a) entire 2009-2016 period; and (b) average for each day of year. Names correspond to Table 2.

## 4 Discussion

### 4.1 Importance of groundwater flow

Three lines of evidence demonstrate that heat transport via groundwater flow is a key control over permafrost response to fire which 1D modeling approaches are unable to capture.



First, for a given set of parameters, active layer thickness is greater in simulations including groundwater flow (2D domain) compared to simulations neglecting groundwater flow (1D domain), indicating that heat transport via advection enhances permafrost thaw relative to conduction-dominated simulations (Figures 3 and 4). Second, including groundwater flow increases the relative importance of hydraulic properties (soil permeability) and decreases the relative importance of thermal properties (soil thermal conductivity), indicating that subsurface heat transport by advection is of greater importance than heat transport by conduction (Figures 3 and 4). Third, model calibration and validation performance is better in the 2D simulations where groundwater flow is included compared to the 1D simulations where groundwater flow is ignored (Figure 5), indicating that including groundwater flow is a more accurate representation of real-world conditions. Combined, these results indicate that lateral heat transport through the active layer via groundwater flow is an important but underappreciated component of post-fire permafrost dynamics.

While previous work has shown that heat transport via lateral groundwater flow can be a positive feedback to permafrost degradation (e.g. Bense et al., 2009, 2012; Connon et al., 2014; Kurylyk et al., 2016; McKenzie & Voss, 2013), this is the first study to demonstrate that advective heat transport is key component of the permafrost response to fire. Importantly, it suggests that spatial variability in the ecohydrological response to fire, a key research priority for disturbance hydrology (Mirus et al., 2017), may be in part driven by groundwater flow which enhances permafrost degradation in lowland areas (Figure 7). Based on our results, we suggest that the degree to which fire effects can be transported laterally via groundwater flow are strongly dependent on post-fire hydraulic gradients and soil properties. Given that both the vertical water balance and soil hydraulic properties may be modified by fire (Kettridge et al., 2012, 2017; Lukenbach et al., 2016; Semenova et al., 2015; Sherwood et al., 2013; Thompson et al., 2014; Thompson & Waddington, 2013), this represents a potential post-fire feedback which merits further investigation.

#### *4.2 Active layer thickness response to water and energy balance changes*

We also demonstrate that changes to the water and energy balance have opposite effects on permafrost thaw depth. Changes to the energy balance increase both conductive and advective energy transport into the subsurface by increasing near-surface soil temperatures which act as an upper boundary to the system (Figure 2), leading to an increase in active layer thickness in both SB and SB<sub>E</sub> scenarios relative to the UB scenario (Figure 6). In contrast, changes to the water balance lead to a reduction in groundwater recharge, which reduces advective heat transport and decreases active layer thickness in the SB<sub>W</sub> scenario relative to the UB scenario (Figure 6).

Our results indicate that changes to the energy balance are the dominant control over the thickness of the active layer following fire as evidenced by the similarity in thaw depth between simulations for the SB site and simulations with only changes to the energy balance (SB<sub>E</sub>) (Figure 6, 7). While the dominance of energy balance changes may seem to contradict the strong sensitivity of modeled thaw dynamics to hydrological parameters (Figures 3 and 4), these results are reconciled by noting that heat transport via advection is a function of both the energy content of groundwater (a function of soil temperature) and the magnitude of groundwater flow (a function of recharge and active layer thickness). Therefore, changes in the energy balance can be the dominant driver of permafrost thaw dynamics as observed in previous studies (Brown et al., 2016), even where groundwater flow is an important process. As warming in high-latitude

regions shifts the timing and magnitude of spring snowmelt, changes in to the water balance may increase in importance (Bring et al., 2016; Lique et al., 2016).

In contrast, changes to the water balance are the dominant control over spatial variability in active layer thickness as evidenced by greater lateral heterogeneity in active layer thickness in simulations with higher groundwater recharge rates (UB, SB<sub>E</sub>) (Figure 7). This is consistent with field observations showing a decrease in the relative variability of thaw depth following fire (Figure 7b-c). While our study focused on a continuous permafrost environment, thaw in lowland areas may be particularly important in areas of discontinuous permafrost where it is likely to increase subsurface hydrologic connectivity which can induce ecologically significant land cover transitions (Connon et al., 2014; Kurylyk et al., 2016; Quinton et al., 2011).

#### *4.3 Baseflow response to water and energy balance changes*

We show that the supply of water (groundwater recharge) is the key control over post-fire changes in baseflow (Figure 8), leading to up to ~50% decreases in annual groundwater discharge in the SB and SB<sub>W</sub> scenarios. Changes in transmissivity appear to have little effect, as the SB<sub>E</sub> scenario which had the largest increase in active layer thickness (Figures 6, 7) has a negligible change in groundwater discharge to the stream under the conditions simulated (Figure 8). Changes in recharge alone are not sufficient to explain the simulated 50% decreases in groundwater discharge, as fire led to only a 40% reduction in groundwater recharge (Figure 2). Therefore, we suggest that a weakening of the hydraulic gradient following fire, as evidenced by the reduced lateral heterogeneity in active layer thickness (Figure 7a), may also be an important driver of changes in baseflow following fire.

Relatively little work has examined changes in groundwater-surface water interactions following fire in permafrost environments. In Alaska, post-fire flow during rain events was enhanced by the increased thickness of the active layer (Petroni et al., 2007). While our study does not examine response to individual precipitation events, the observed increases in transmissivity resulting from fire shown here (e.g. Figure 7a) provide a mechanism for these increases in stormflow. In contrast, in our simulations lower water inputs led to a net decrease in groundwater discharge to streams. At larger scales, previous work has shown that forest fires cause a slight increase in streamflow, though this signal is small relative to changes in atmospheric moisture transport (McClelland et al., 2004).

We suggest that the impacts of fire on groundwater discharge to streams depend strongly on local site characteristics, given the substantial uncertainty regarding post-fire changes to the water and energy balance. For instance, previous work has demonstrated that in settings where permafrost thaw leads to enhanced subsurface connectivity (e.g. the talik grows deep enough to connect to a subpermafrost aquifer), groundwater flow processes can exert a major control (Bense et al., 2012). Thus, the impacts of fire on baseflow may be stronger in regions of discontinuous permafrost with more dynamic changes in hydrologic connectivity (Connon et al., 2014, 2015; Walvoord et al., 2012). Furthermore, at our study site fire was associated with an increase in evapotranspiration and concomitant reduction in groundwater recharge (Rocha & Shaver, 2011b); work elsewhere has documented both increases (Thompson et al., 2014) and decreases (Liu et al., 2005) in evapotranspiration following fire in cold regions, indicating that advances to our understanding of the land surface water and energy balance are necessary to improve boundary representation in subsurface models.



#### 4.4 Study limitations

Despite the strong model performance when compared to field observations (Figure 5), there are several limitations to our approach which may affect our results. First, freeze/thaw processes in our model only consider freezing of water within existing pore space, and therefore processes such as thermokarst development and ice lensing are not simulated. Second, the archetypal modeling approach we use here simulates saturated flow with homogeneous subsurface properties; variably saturated processes may be important, particularly in high-porosity soils in which air-filled pore space can act as a thermal buffer (Kettridge et al., 2012). Third, our model is only of the subsurface, and therefore ponding at the land surface cannot occur if there is insufficient infiltration capacity; this likely reduces both the quantity and duration of groundwater recharge, particularly during spring snowmelt, and may dampen effects of changes in the water balance. Finally, our specified boundary condition intended to represent a streambed is simplified and does not include temporal dynamics (e.g. high water levels during spring freshet, seasonal changes in temperature) which may influence stream-aquifer interactions. Additional field measurements such as stream stage, stream temperature, and water table gradient in the hillslope areas may help resolve some of these uncertainties and aid in the construction of a site-specific model.

While our modeling approach may neglect some locally-important processes, the objective of our research was to isolate the effects of groundwater flow on post-fire permafrost distribution. Our archetypal approach to groundwater modeling provides information about the fundamental processes controlling system dynamics, and therefore provides more generalizable information than highly parameterized models while also providing insight into the system of interest (Ge et al., 2011; Gleeson et al., 2016; Niswonger et al., 2017; Voss, 2011a, 2011b; Zipper et al., 2017a). By leaving out these processes, we are better able to isolate the role of groundwater, providing a more generalized understanding of flow processes in variably frozen porous media, which physical properties and model parameters most strongly influence the response subsurface processes to fire, and how fire-induced changes are able to propagate laterally through groundwater flow.

## 5 Conclusions

In this study, we quantified the importance of groundwater flow to permafrost thaw following fire. Our results demonstrate that hydrogeological processes are a key control over permafrost dynamics following fire, and that neglecting lateral water and heat transport may lead to overestimation of the importance of thermal properties. We also show that an increase in energy input to the subsurface following fire is the primary driver of increases in active layer thickness, and permafrost thaw is enhanced by advective heat transport via groundwater flow. However, changes to the water balance are the key control over the post-fire spatial heterogeneity in thaw depth and groundwater discharge to surface water features. These results show that groundwater flow and associated processes must be considered to understand both terrestrial and hydrological response to fire in permafrost settings.

## Acknowledgments and Data

SCZ, PLH, and JMM were funded by the Natural Sciences and Engineering Research Council of Canada (NSERC) and the McGill University Trottier Institute for Science and Public Policy. AVR and data collection were funded by NSF grant #1556772 to the University of Notre Dame.

We appreciate discussions with Tom Gleeson, Yueyang Jiang, and Barret Kurylyk. Anaktuvuk River data sets were provided by the Arctic LTER (Rocha and Shaver, 2015; Shaver and Rocha, 2015a-o). This material is based upon work supported by the National Science Foundation under grants #DEB-981022, 9211775, 8702328; #OPP-9911278, 9911681, 9732281, 9615411, 9615563, 9615942, 9615949, 9400722, 9415411, 9318529; #BSR 9019055, 8806635, 8507493. Meteorological datasets were provided by the Toolik Field Station Environmental Data Center (Environmental Data Center Team, 2017) based upon work supported by the National Science Foundation under grants #455541 and 1048361. All analyses were performed using R 3.4.0 (R Core Team, 2017) and graphics made using ggplot2 (Wickham, 2009) and InkScape (The Inkscape Team, 2015). Field data, model input files, and analysis scripts will be made available on FigShare at article acceptance.

## References

- Bense, V. F., Ferguson, G., & Kooi, H. (2009). Evolution of shallow groundwater flow systems in areas of degrading permafrost. *Geophysical Research Letters*, *36*(22), L22401. <https://doi.org/10.1029/2009GL039225>
- Bense, V. F., Kooi, H., Ferguson, G., & Read, T. (2012). Permafrost degradation as a control on hydrogeological regime shifts in a warming climate. *Journal of Geophysical Research-Earth Surface*, *117*, F03036. <https://doi.org/10.1029/2011JF002143>
- Bret-Harte, M. S., Mack, M. C., Shaver, G. R., Huebner, D. C., Johnston, M., Mojica, C. A., ... Reiskind, J. A. (2013). The response of Arctic vegetation and soils following an unusually severe tundra fire. *Philosophical Transactions of the Royal Society B-Biological Sciences*, *368*(1624), UNSP 20120490. <https://doi.org/10.1098/rstb.2012.0490>
- Bring, A., Fedorova, I., Dibike, Y., Hinzman, L., Mard, J., Mernild, S. H., ... Woo, M.-K. (2016). Arctic terrestrial hydrology: A synthesis of processes, regional effects, and research challenges. *Journal of Geophysical Research-Biogeosciences*, *121*(3), 621–649. <https://doi.org/10.1002/2015JG003131>
- Brown, D. R. N., Jorgenson, M. T., Kielland, K., Verbyla, D. L., Prakash, A., & Koch, J. C. (2016). Landscape Effects of Wildfire on Permafrost Distribution in Interior Alaska Derived from Remote Sensing. *Remote Sensing*, *8*(8), 654. <https://doi.org/10.3390/rs8080654>
- Brown, D. R. N., Jorgenson, M. T., Douglas, T. A., Romanovsky, V. E., Kielland, K., Hiemstra, C., ... Ruess, R. W. (2015). Interactive effects of wildfire and climate on permafrost degradation in Alaskan lowland forests. *Journal of Geophysical Research-Biogeosciences*, *120*(8), 1619–1637. <https://doi.org/10.1002/2015JG003033>
- Campbell, G. S., & Norman, J. M. (2000). *An Introduction to Environmental Biophysics* (2nd ed.). Springer.
- Carsel, R. F., & Parrish, R. S. (1988). Developing joint probability-distributions of soil-water retention characteristics. *Water Resources Research*, *24*(5), 755–769. <https://doi.org/10.1029/WR024i005p00755>
- Clow, G. D. (2014). Global Terrestrial Network for Permafrost - Seabee. Retrieved February 27, 2017, from <http://gtnpdatabase.org/boreholes/view/812>
- Connon, R. F., Quinton, W. L., Craig, J. R., & Hayashi, M. (2014). Changing hydrologic connectivity due to permafrost thaw in the lower Liard River valley, NWT, Canada. *Hydrological Processes*, *28*(14), 4163–4178. <https://doi.org/10.1002/hyp.10206>
- Connon, R. F., Quinton, W. L., Craig, J. R., Hanisch, J., & Sonnentag, O. (2015). The hydrology of interconnected bog complexes in discontinuous permafrost terrains. *Hydrological Processes*, *29*(18), 3831–3847. <https://doi.org/10.1002/hyp.10604>
- De Baets, S., van de Weg, M. J., Lewis, R., Steinberg, N., Meersmans, J., Quine, T. A., ... Hartley, I. P. (2016). Investigating the controls on soil organic matter decomposition in tussock tundra soil and permafrost after fire. *Soil Biology and Biochemistry*, *99*, 108–116. <https://doi.org/10.1016/j.soilbio.2016.04.020>

- Environmental Data Center Team. (2017). Meteorological Monitoring program at Toolik, Alaska. Toolik Field Station, Institute of Arctic Biology, University of Alaska Fairbanks, Fairbanks, AK 99775. Retrieved March 27, 2017, from [http://toolik.alaska.edu/edc/abiotic\\_monitoring/data\\_query.php](http://toolik.alaska.edu/edc/abiotic_monitoring/data_query.php)
- Evans, S. G., & Ge, S. (2017). Contrasting hydrogeologic responses to warming in permafrost and seasonally frozen ground hillslopes. *Geophysical Research Letters*, *44*(4), 2016GL072009. <https://doi.org/10.1002/2016GL072009>
- Flannigan, M. D., Logan, K. A., Amiro, B. D., Skinner, W. R., & Stocks, B. J. (2005). Future area burned in Canada. *Climatic Change*, *72*(1–2), 1–16. <https://doi.org/10.1007/s10584-005-5935-y>
- Fuka, D., Walter, M., Archibald, J., Steenhuis, J., & Easton, Z. (2014). EcoHydRology: A community modeling foundation for Eco-Hydrology (Version 0.4.12). Retrieved from <https://CRAN.R-project.org/package=EcoHydRology>
- Ge, S., McKenzie, J., Voss, C., & Wu, Q. (2011). Exchange of groundwater and surface-water mediated by permafrost response to seasonal and long term air temperature variation. *Geophysical Research Letters*, *38*(14), L14402. <https://doi.org/10.1029/2011GL047911>
- Gleeson, T., Befus, K. M., Jasechko, S., Luijendijk, E., & Cardenas, M. B. (2016). The global volume and distribution of modern groundwater. *Nature Geoscience*, *9*(2), 161–167. <https://doi.org/10.1038/ngeo2590>
- Gupta, H. V., Kling, H., Yilmaz, K. K., & Martinez, G. F. (2009). Decomposition of the mean squared error and NSE performance criteria: Implications for improving hydrological modelling. *Journal of Hydrology*, *377*(1), 80–91. <https://doi.org/10.1016/j.jhydrol.2009.08.003>
- Higuera, P. E., Brubaker, L. B., Anderson, P. M., Brown, T. A., Kennedy, A. T., & Hu, F. S. (2008). Frequent Fires in Ancient Shrub Tundra: Implications of Paleorecords for Arctic Environmental Change. *PLoS ONE*, *3*(3), e0001744. <https://doi.org/10.1371/journal.pone.0001744>
- Hu, F. S., Higuera, P. E., Walsh, J. E., Chapman, W. L., Duffy, P. A., Brubaker, L. B., & Chipman, M. L. (2010). Tundra burning in Alaska: Linkages to climatic change and sea ice retreat. *Journal of Geophysical Research: Biogeosciences*, *115*(G4), G04002. <https://doi.org/10.1029/2009JG001270>
- Hu, F. S., Higuera, P. E., Duffy, P., Chipman, M. L., Rocha, A. V., Young, A. M., ... Dietze, M. C. (2015). Arctic tundra fires: natural variability and responses to climate change. *Frontiers in Ecology and the Environment*, *13*(7), 369–377. <https://doi.org/10.1890/150063>
- Iwahana, G., Harada, K., Uchida, M., Tsuyuzaki, S., Saito, K., Narita, K., ... Hinzman, L. D. (2016). Geomorphological and geochemistry changes in permafrost after the 2002 tundra wildfire in Kougarak, Seward Peninsula, Alaska. *Journal of Geophysical Research: Earth Surface*, *121*(9), 2016JF003921. <https://doi.org/10.1002/2016JF003921>
- Jafarov, E. E., Romanovsky, V. E., Genet, H., McGuire, A. D., & Marchenko, S. S. (2013). The effects of fire on the thermal stability of permafrost in lowland and upland black spruce forests of interior Alaska in a changing climate. *Environmental Research Letters*, *8*(3), 035030. <https://doi.org/10.1088/1748-9326/8/3/035030>
- Jiang, Y., Rastetter, E. B., Shaver, G. R., Rocha, A. V., Zhuang, Q., & Kwiatkowski, B. L. (2017). Modeling long-term changes in tundra carbon balance following wildfire, climate change, and potential nutrient addition. *Ecological Applications*, *27*(1), 105–117. <https://doi.org/10.1002/eap.1413>
- Jiang, Y., Zhuang, Q., & O'Donnell, J. A. (2012). Modeling thermal dynamics of active layer soils and near-surface permafrost using a fully coupled water and heat transport model. *Journal of Geophysical Research: Atmospheres*, *117*(D11), D11110. <https://doi.org/10.1029/2012JD017512>
- Jiang, Y., Rastetter, E. B., Rocha, A. V., Pearce, A. R., Kwiatkowski, B. L., & Shaver, G. . . (2015a). Modeling carbon–nutrient interactions during the early recovery of tundra after fire. *Ecological Applications*, *25*(6), 1640–1652. <https://doi.org/10.1890/14-1921.1>
- Jiang, Y., Rocha, A. V., O'Donnell, J. A., Drysdale, J. A., Rastetter, E. B., Shaver, G. R., & Zhuang, Q. (2015b). Contrasting soil thermal responses to fire in Alaskan tundra and boreal forest. *Journal of Geophysical Research-Earth Surface*, *120*(2), 363–378. <https://doi.org/10.1002/2014JF003180>

- Jones, B. M., Kolden, C. A., Jandt, R., Abatzoglou, J. T., Urban, F., & Arp, C. D. (2009). Fire Behavior, Weather, and Burn Severity of the 2007 Anaktuvuk River Tundra Fire, North Slope, Alaska. *Arctic, Antarctic, and Alpine Research*, 41(3), 309–316. <https://doi.org/10.1657/1938-4246-41.3.309>
- Kasischke, E. S., & Johnstone, J. F. (2005). Variation in postfire organic layer thickness in a black spruce forest complex in interior Alaska and its effects on soil temperature and moisture. *Canadian Journal of Forest Research-Revue Canadienne De Recherche Forestiere*, 35(9), 2164–2177. <https://doi.org/10.1139/X05-159>
- Kasischke, E. S., Bourgeau-Chavez, L. L., & Johnstone, J. F. (2007). Assessing spatial and temporal variations in surface soil moisture in fire-disturbed black spruce forests in Interior Alaska using spaceborne synthetic aperture radar imagery - Implications for post-fire tree recruitment. *Remote Sensing of Environment*, 108(1), 42–58. <https://doi.org/10.1016/j.rse.2006.10.020>
- Kettridge, N., Thompson, D. K., & Waddington, J. M. (2012). Impact of wildfire on the thermal behavior of northern peatlands: Observations and model simulations. *Journal of Geophysical Research: Biogeosciences*, 117(G2), G02014. <https://doi.org/10.1029/2011JG001910>
- Kettridge, N., Lukenbach, M. C., Hokanson, K. J., Hopkinson, C., Devito, K. J., Petrone, R. M., ... Waddington, J. M. (2017). Low Evapotranspiration Enhances the Resilience of Peatland Carbon Stocks to Fire. *Geophysical Research Letters*, 44(18), 2017GL074186. <https://doi.org/10.1002/2017GL074186>
- Kurylyk, B. L., Hayashi, M., Quinton, W. L., McKenzie, J. M., & Voss, C. I. (2016). Influence of vertical and lateral heat transfer on permafrost thaw, peatland landscape transition, and groundwater flow. *Water Resources Research*, 52(2), 1286–1305. <https://doi.org/10.1002/2015WR018057>
- Liljedahl, A. K., Hinzman, L. D., Kane, D. L., Oechel, W. C., Tweedie, C. E., & Zona, D. (2017). Tundra water budget and implications of precipitation underestimation. *Water Resources Research*, 53(8), 6472–6486. <https://doi.org/10.1002/2016WR020001>
- Lique, C., Holland, M. M., Dibike, Y. B., Lawrence, D. M., & Screen, J. A. (2016). Modeling the Arctic freshwater system and its integration in the global system: Lessons learned and future challenges. *Journal of Geophysical Research-Biogeosciences*, 121(3), 540–566. <https://doi.org/10.1002/2015JG003120>
- Liu, H. P., Randerson, J. T., Lindfors, J., & Chapin, F. S. (2005). Changes in the surface energy budget after fire in boreal ecosystems of interior Alaska: An annual perspective. *Journal of Geophysical Research-Atmospheres*, 110(D13), D13101. <https://doi.org/10.1029/2004JD005158>
- Lukenbach, M. C., Devito, K. J., Kettridge, N., Petrone, R. M., & Waddington, J. M. (2016). Burn severity alters peatland moss water availability: implications for post-fire recovery. *Ecohydrology*, 9(2), 341–353. <https://doi.org/10.1002/eco.1639>
- Mack, M. C., Bret-Harte, M. S., Hollingsworth, T. N., Jandt, R. R., Schuur, E. A. G., Shaver, G. R., & Verbyla, D. L. (2011). Carbon loss from an unprecedented Arctic tundra wildfire. *Nature*, 475(7357), 489–492. <https://doi.org/10.1038/nature10283>
- McClelland, J. W., Holmes, R. M., Peterson, B. J., & Stieglitz, M. (2004). Increasing river discharge in the Eurasian Arctic: Consideration of dams, permafrost thaw, and fires as potential agents of change. *Journal of Geophysical Research-Atmospheres*, 109(D18), D18102. <https://doi.org/10.1029/2004JD004583>
- McKenzie, J. M., Voss, C. I., & Siegel, D. I. (2007). Groundwater flow with energy transport and water–ice phase change: Numerical simulations, benchmarks, and application to freezing in peat bogs. *Advances in Water Resources*, 30(4), 966–983. <https://doi.org/10.1016/j.advwatres.2006.08.008>
- McKenzie, J. M., & Voss, C. I. (2013). Permafrost thaw in a nested groundwater-flow system. *Hydrogeology Journal*, 21(1), 299–316. <https://doi.org/10.1007/s10040-012-0942-3>
- Minsley, B. J., Pastick, N. J., Wylie, B. K., Brown, D. R. N., & Kass, M. A. (2016). Evidence for nonuniform permafrost degradation after fire in boreal landscapes. *Journal of Geophysical Research-Earth Surface*, 121(2), 320–335. <https://doi.org/10.1002/2015JF003781>
- Mirus, B. B., Ebel, B. A., Mohr, C. H., & Zegre, N. (2017). Disturbance Hydrology: Preparing for an Increasingly Disturbed Future. *Water Resources Research*. <https://doi.org/10.1002/2017WR021084>

- Naasz, R., Michel, J.-C., & Charpentier, S. (2005). Measuring Hysteretic Hydraulic Properties of Peat and Pine Bark using a Transient Method. *Soil Science Society of America Journal*, 69(1), 13–22. <https://doi.org/10.2136/sssaj2005.0013>
- Nash, J. E., & Sutcliffe, J. V. (1970). River flow forecasting through conceptual models part I — A discussion of principles. *Journal of Hydrology*, 10(3), 282–290. [https://doi.org/10.1016/0022-1694\(70\)90255-6](https://doi.org/10.1016/0022-1694(70)90255-6)
- Niswonger, R. G., Morway, E. D., Triana, E., & Huntington, J. L. (2017). Managed aquifer recharge through off-season irrigation in agricultural regions. *Water Resources Research*, 53(8), 6970–6992. <https://doi.org/10.1002/2017WR020458>
- Petrone, K. C., Hinzman, L. D., Shibata, H., Jones, J. B., & Boone, R. D. (2007). The influence of fire and permafrost on sub-arctic stream chemistry during storms. *Hydrological Processes*, 21(4), 423–434. <https://doi.org/10.1002/hyp.6247>
- Quinton, W. L., Hayashi, M., & Chasmer, L. E. (2011). Permafrost-thaw-induced land-cover change in the Canadian subarctic: implications for water resources. *Hydrological Processes*, 25(1), 152–158. <https://doi.org/10.1002/hyp.7894>
- R Core Team. (2017). R: A language and environment for statistical computing (Version 3.4.0). Vienna, Austria: R Foundation for Statistical Computing. Retrieved from <https://www.R-project.org/>
- Rocha, A. V., Shaver, G. R., & Hobbie, J. (2008a). AmeriFlux US-An1 Anaktuvuk River Moderate Burn. Retrieved February 27, 2017, from <http://dx.doi.org/10.17190/AMF/1246143>
- Rocha, A. V., Shaver, G. R., & Hobbie, J. (2008b). AmeriFlux US-An1 Anaktuvuk River Severe Burn. Retrieved February 27, 2017, from <http://dx.doi.org/10.17190/AMF/1246142>
- Rocha, A. V., Shaver, G. R., & Hobbie, J. (2008c). AmeriFlux US-An1 Anaktuvuk River Unburned. Retrieved February 27, 2017, from <http://dx.doi.org/10.17190/AMF/1246144>
- Rocha, A. V., & Shaver, G. R. (2009). Advantages of a two band EVI calculated from solar and photosynthetically active radiation fluxes. *Agricultural and Forest Meteorology*, 149(9), 1560–1563. <https://doi.org/10.1016/j.agrformet.2009.03.016>
- Rocha, A. V., & Shaver, G. R. (2011a). Burn severity influences postfire CO<sub>2</sub> exchange in arctic tundra. *Ecological Applications*, 21(2), 477–489. <https://doi.org/10.1890/10-0255.1>
- Rocha, A. V., & Shaver, G. R. (2011b). Postfire energy exchange in arctic tundra: the importance and climatic implications of burn severity. *Global Change Biology*, 17(9), 2831–2841. <https://doi.org/10.1111/j.1365-2486.2011.02441.x>
- Rocha, A. V., & Shaver, G. R. (2015, December 14). Anaktuvuk River fire scar thaw depth measurements during the 2008 to 2014 growing season. Retrieved February 8, 2017, from <http://dx.doi.org/10.6073/pasta/93121fc86e6fbcf88de4a9350609aed6>
- Romanovsky, V. E., Ping, C.-L., Seybold, C., & Harms, D. (2017). Toolik Soil Climate Station. Retrieved March 27, 2017, from [https://www.nrcs.usda.gov/wps/portal/nrcs/detail/soils/home/?cid=NRCS142P2\\_053712](https://www.nrcs.usda.gov/wps/portal/nrcs/detail/soils/home/?cid=NRCS142P2_053712)
- Schwärzel, K., Šimůnek, J., Stoffregen, H., Wessolek, G., Genuchten, V., & Th, M. (2006). Estimation of the Unsaturated Hydraulic Conductivity of Peat Soils. *Vadose Zone Journal*, 5(2), 628–640. <https://doi.org/10.2136/vzj2005.0061>
- Semenova, O., Lebedeva, L., Volkova, N., Korenev, I., Forkel, M., Eberle, J., & Urban, M. (2015). Detecting immediate wildfire impact on runoff in a poorly-gauged mountainous permafrost basin. *Hydrological Sciences Journal-Journal Des Sciences Hydrologiques*, 60(7–8), 1225–1241. <https://doi.org/10.1080/02626667.2014.959960>
- Serbin, S. P., Singh, A., McNeil, B. E., Kingdon, C. C., & Townsend, P. A. (2014). Spectroscopic determination of leaf morphological and biochemical traits for northern temperate and boreal tree species. *Ecological Applications*, 24(7), 1651–1669. <https://doi.org/10.1890/13-2110.1>

- Shaver, G. R., & Rocha, A. V. (2015a, December 14). Anaktuvuk River Burn Eddy Flux Measurements, 2008 Moderate Site, North Slope Alaska. Retrieved February 8, 2017, from <http://dx.doi.org/10.6073/pasta/19e3802d6738c4b30cf09188a2551b10>
- Shaver, G. R., & Rocha, A. V. (2015b, December 14). Anaktuvuk River Burn Eddy Flux Measurements, 2008 Severe Site, North Slope Alaska. Retrieved February 8, 2017, from <http://dx.doi.org/10.6073/pasta/724bd68e01ee9a59b05cdee5cfa14bbd>
- Shaver, G. R., & Rocha, A. V. (2015c, December 14). Anaktuvuk River Burn Eddy Flux Measurements, 2008 Unburned Site, North Slope Alaska. Retrieved February 8, 2017, from <http://dx.doi.org/10.6073/pasta/48f728d2fe75541c8f4f6827ce8dc039>
- Shaver, G. R., & Rocha, A. V. (2015d, December 14). Anaktuvuk River Burn Eddy Flux Measurements, 2009 Moderate Site, North Slope Alaska. Retrieved February 8, 2017, from <http://dx.doi.org/10.6073/pasta/3d912564439309bdf17bc75866179312>
- Shaver, G. R., & Rocha, A. V. (2015e, December 14). Anaktuvuk River Burn Eddy Flux Measurements, 2009 Severe Site, North Slope Alaska. Retrieved February 8, 2017, from <http://dx.doi.org/10.6073/pasta/5554a6eda8082f933709e547811b85dc>
- Shaver, G. R., & Rocha, A. V. (2015f, December 14). Anaktuvuk River Burn Eddy Flux Measurements, 2009 Unburned Site, North Slope Alaska. Retrieved February 8, 2017, from <http://dx.doi.org/10.6073/pasta/aeb3845bf779ca10f13930e1d6c90105>
- Shaver, G. R., & Rocha, A. V. (2015g, December 14). Anaktuvuk River Burn Eddy Flux Measurements, 2010 Moderate Site, North Slope Alaska. Retrieved February 8, 2017, from <http://dx.doi.org/10.6073/pasta/abee3157f007a794edb3414e1280d71b>
- Shaver, G. R., & Rocha, A. V. (2015h, December 14). Anaktuvuk River Burn Eddy Flux Measurements, 2010 Severe Site, North Slope Alaska. Retrieved February 8, 2017, from <http://dx.doi.org/10.6073/pasta/2330a47db633130f0972bc134e714066>
- Shaver, G. R., & Rocha, A. V. (2015i, December 14). Anaktuvuk River Burn Eddy Flux Measurements, 2010 Unburned Site, North Slope Alaska. Retrieved February 8, 2017, from <http://dx.doi.org/10.6073/pasta/ff790bd426b262aa7d818ad7f0b2d2a4>
- Shaver, G. R., & Rocha, A. V. (2015j, December 14). Anaktuvuk River Burn Eddy Flux Measurements, 2011 Moderate Site, North Slope Alaska. Retrieved February 8, 2017, from <http://dx.doi.org/10.6073/pasta/f7e7d023fbac22d83ad0c2e4ce191650>
- Shaver, G. R., & Rocha, A. V. (2015k, December 14). Anaktuvuk River Burn Eddy Flux Measurements, 2011 Severe Site, North Slope Alaska. Retrieved February 8, 2017, from <http://dx.doi.org/10.6073/pasta/d384b812a12e5cfa7fdbb4032cf1abb2>
- Shaver, G. R., & Rocha, A. V. (2015l, December 14). Anaktuvuk River Burn Eddy Flux Measurements, 2011 Unburned Site, North Slope Alaska. Retrieved February 8, 2017, from <http://dx.doi.org/10.6073/pasta/913d3843eb71f27bac3f9c97df61573e>
- Shaver, G. R., & Rocha, A. V. (2015m, December 14). Anaktuvuk River Burn Eddy Flux Measurements, 2012 Moderate Site, North Slope Alaska. Retrieved February 8, 2017, from <http://dx.doi.org/10.6073/pasta/b5c015dbf57ba3b3ec3ee1d95a663fc5>
- Shaver, G. R., & Rocha, A. V. (2015n, December 14). Anaktuvuk River Burn Eddy Flux Measurements, 2012 Severe Site, North Slope Alaska. Retrieved February 8, 2017, from <http://dx.doi.org/10.6073/pasta/ed412a2a1940af95ab4611212200a5c5>
- Shaver, G. R., & Rocha, A. V. (2015o, December 14). Anaktuvuk River Burn Eddy Flux Measurements, 2012 Unburned Site, North Slope Alaska. Retrieved February 8, 2017, from <http://dx.doi.org/10.6073/pasta/67188afe29827f8b3c0277753b2a956a>
- Sherwood, J. H., Kettridge, N., Thompson, D. K., Morris, P. J., Silins, U., & Waddington, J. M. (2013). Effect of drainage and wildfire on peat hydrophysical properties. *Hydrological Processes*, 27(13), 1866–1874. <https://doi.org/10.1002/hyp.9820>

- da Silva, F. F., Wallach, R., & Chen, Y. (1993). Hydraulic properties of sphagnum peat moss and tuff (scoria) and their potential effects on water availability. *Plant and Soil*, *154*(1), 119–126. <https://doi.org/10.1007/BF00011080>
- Smith, S. L., Riseborough, D. W., & Bonnaventure, P. P. (2015). Eighteen Year Record of Forest Fire Effects on Ground Thermal Regimes and Permafrost in the Central Mackenzie Valley, NWT, Canada. *Permafrost and Periglacial Processes*, *26*(4), 289–303. <https://doi.org/10.1002/ppp.1849>
- The Inkscape Team. (2015). Inkscape (Version 0.91). Retrieved from <https://inkscape.org/en/>
- Thompson, D. K., & Waddington, J. M. (2013). Peat properties and water retention in boreal forested peatlands subject to wildfire. *Water Resources Research*, *49*(6), 3651–3658. <https://doi.org/10.1002/wrcr.20278>
- Thompson, D. K., Benscoter, B. W., & Waddington, J. M. (2014). Water balance of a burned and unburned forested boreal peatland. *Hydrological Processes*, *28*(24), 5954–5964. <https://doi.org/10.1002/hyp.10074>
- Treat, C. C., Wisser, D., Marchenko, S., & Frohling, S. (2013). Modelling the effects of climate change and disturbance on permafrost stability in northern organic soils. *Mires and Peat*, *12*, 2.
- Voss, C. I. (2011a). Editor's message: Groundwater modeling fantasies —part 1, adrift in the details. *Hydrogeology Journal*, *19*(7), 1281–1284. <https://doi.org/10.1007/s10040-011-0789-z>
- Voss, C. I. (2011b). Editor's message: Groundwater modeling fantasies—part 2, down to earth. *Hydrogeology Journal*, *19*(8), 1455–1458. <https://doi.org/10.1007/s10040-011-0790-6>
- Voss, C. I., & Provost, A. M. (2010). *SUTRA: A Model for Saturated-Unsaturated Variable-Density Ground-Water Flow with Solute or Energy Transport* (No. Water Resources Investigations Report 02-4231). Reston VA: U.S. Geological Survey.
- Walter, M. T., Brooks, E. S., McCool, D. K., King, L. G., Molnau, M., & Boll, J. (2005). Process-based snowmelt modeling: does it require more input data than temperature-index modeling? *Journal of Hydrology*, *300*(1), 65–75. <https://doi.org/10.1016/j.jhydrol.2004.05.002>
- Walvoord, M. A., & Kurylyk, B. L. (2016). Hydrologic Impacts of Thawing Permafrost-A Review. *Vadose Zone Journal*, *15*(6). <https://doi.org/10.2136/vzj2016.01.0010>
- Walvoord, M. A., Voss, C. I., & Wellman, T. P. (2012). Influence of permafrost distribution on groundwater flow in the context of climate-driven permafrost thaw: Example from Yukon Flats Basin, Alaska, United States. *Water Resources Research*, *48*(7), W07524. <https://doi.org/10.1029/2011WR011595>
- Wellman, T. P., Voss, C. I., & Walvoord, M. A. (2013). Impacts of climate, lake size, and supra- and sub-permafrost groundwater flow on lake-talik evolution, Yukon Flats, Alaska (USA). *Hydrogeology Journal*, *21*(1), 281–298. <https://doi.org/10.1007/s10040-012-0941-4>
- Wickham, H. (2009). *ggplot2: Elegant Graphics for Data Analysis*. Springer-Verlag New York. Retrieved from <http://ggplot2.org>
- Wood, S. N. (2003). Thin-plate regression splines. *Journal of the Royal Statistical Society (B)*, *65*(1), 95–114.
- Wood, S. N. (2011). Fast stable restricted maximum likelihood and marginal likelihood estimation of semiparametric generalized linear models. *Journal of the Royal Statistical Society (B)*, *73*(1), 3–36.
- Wood, S. N. (2017). *Generalized Additive Models: An Introduction with R (2nd edition)*. Chapman and Hall/CRC.
- Wrona, F. J., Johansson, M., Culp, J. M., Jenkins, A., Mård, J., Myers-Smith, I. H., ... Wookey, P. A. (2016). Transitions in Arctic ecosystems: Ecological implications of a changing hydrological regime. *Journal of Geophysical Research: Biogeosciences*, *121*(3), 2015JG003133. <https://doi.org/10.1002/2015JG003133>
- Yi, S., McGuire, A. D., Harden, J., Kasischke, E. S., Manies, K., Hinzman, L., ... Kim, Y. (2009). Interactions between soil thermal and hydrological dynamics in the response of Alaska ecosystems to fire disturbance. *Journal of Geophysical Research-Biogeosciences*, *114*, G02015. <https://doi.org/10.1029/2008JG000841>
- Zambrano-Bigiarini, M. (2014). hydroGOF: Goodness-of-fit functions for comparison of simulated and observed hydrological time series (Version 0.3-8). Retrieved from <https://CRAN.R-project.org/package=hydroGOF>

- Zhang, Y., Chen, W., & Cihlar, J. (2003). A process-based model for quantifying the impact of climate change on permafrost thermal regimes. *Journal of Geophysical Research: Atmospheres*, 108(D22), 4695. <https://doi.org/10.1029/2002JD003354>
- Zhang, Y., Carey, S. K., Quinton, W. L., Janowicz, J. R., Pomeroy, J. W., & Flerchinger, G. N. (2010). Comparison of algorithms and parameterisations for infiltration into organic-covered permafrost soils. *Hydrology and Earth System Sciences*, 14(5), 729–750. <https://doi.org/10.5194/hess-14-729-2010>
- Zhang, Y., Wolfe, S. A., Morse, P. D., Olthof, I., & Fraser, R. H. (2015). Spatiotemporal impacts of wildfire and climate warming on permafrost across a subarctic region, Canada. *Journal of Geophysical Research-Earth Surface*, 120(11), 2338–2356. <https://doi.org/10.1002/2015JF003679>
- Zhuang, Q., McGuire, A. D., O’Neill, K. P., Harden, J. W., Romanovsky, V. E., & Yarie, J. (2002). Modeling soil thermal and carbon dynamics of a fire chronosequence in interior Alaska. *Journal of Geophysical Research-Atmospheres*, 108(D1), 8147. <https://doi.org/10.1029/2001JD001244>
- Zipper, S. C., Soylu, M. E., Kucharik, C. J., & Loheide II, S. P. (2017a). Quantifying indirect groundwater-mediated effects of urbanization on agroecosystem productivity using MODFLOW-AgroIBIS (MAGI), a complete critical zone model. *Ecological Modelling*, 359, 201–219. <https://doi.org/10.1016/j.ecolmodel.2017.06.002>
- Zipper, S. C., & Loheide, S. P. (2014). Using evapotranspiration to assess drought sensitivity on a subfield scale with HRMET, a high resolution surface energy balance model. *Agricultural and Forest Meteorology*, 197, 91–102. <https://doi.org/10.1016/j.agrformet.2014.06.009>
- Zipper, S. C., Schatz, J., Singh, A., Kucharik, C. J., Townsend, P. A., & Loheide, S. P. (2016). Urban heat island impacts on plant phenology: intra-urban variability and response to land cover. *Environmental Research Letters*, 11(5), 054023. <https://doi.org/10.1088/1748-9326/11/5/054023>
- Zipper, S. C., Schatz, J., Kucharik, C. J., & Loheide, S. P. (2017b). Urban heat island-induced increases in evapotranspirative demand. *Geophysical Research Letters*, 44(2), 2016GL072190. <https://doi.org/10.1002/2016GL072190>